Mutational Analysis of Preamyloid Intermediates: The Role of His-Tyr Interactions in Islet Amyloid Formation

Ling-Hsien Tu,[†] Arnaldo L. Serrano,[‡] Martin T. Zanni,[‡] and Daniel P. Raleigh[†*]
[†]Department of Chemistry, Stony Brook University, Stony Brook, New York; and [‡]Department of Chemistry, University of Wisconsin-Madison, Madison, Wisconsin

ABSTRACT Islet amyloid polypeptide (IAPP or Amylin) is a 37-residue, C-terminally amidated pancreatic hormone, cosecreted with insulin that forms islet amyloid in type 2 diabetes. Islet amyloid formation is complex and characterizing preamyloid oligomers is an important topic because oligomeric intermediates are postulated to be the most toxic species produced during fibril formation. A range of competing models for early oligomers have been proposed. The role of the amidated C-terminus in amyloid formation by IAPP and in stabilizing oligomers is not known. Studies with unamidated IAPP have provided evidence for formation of an antiparallel dimer at pH 5.5, stabilized by stacking of His-18 and Tyr-37, but it is not known if this interaction is formed in the physiological form of the peptide. Analysis of a set of variants with a free and with an amidated C-terminus shows that disrupting the putative His-Tyr interaction accelerates amyloid formation, indicating that it is not essential. Amidation to generate the physiologically relevant form of IAPP accelerates amyloid formation, demonstrating that the advantages conferred by C-terminal amidation outweigh increased amyloidogenicity. The analysis of this variant argues that IAPP is not under strong evolutionary pressure to reduce amyloidogenicity. Analysis of an H18Q mutant of IAPP shows that the charge state of the N-terminus is an important factor controlling the rate of amyloid formation, even though the N-terminal region of IAPP is believed to be flexible in the amyloid fibers.

INTRODUCTION

More than 30 different human diseases involve the deposition of partially ordered protein aggregates known as amyloids (1–3). Although there is no sequence similarity between the proteins involved, all amyloid deposits are rich in β-sheet structure and they share several common features including the ability to bind extrinsic fluorescent dyes such as thioflavin-T (ThT) (4). Islet amyloid polypeptide (IAPP, or amylin), a pancreatic hormone cosecreted with insulin, forms islet amyloid in type 2 diabetes, and leads to β-cell dysfunction and cell death (5–13). Formation of islet amyloid is also believed to contribute significantly to the failure of islet cell transplants (14–16). Islet amyloid formation is complex and not well understood, despite its importance.

The polypeptide is 37 residues in length, contains a disulfide bond between residues 2 and 7, and has an amidated C-terminus, which is required for full biological activity (Fig. 1 *A*) (17). IAPP is considered to be natively unfolded in its monomeric state, but is one of the most amyloidogenic natural sequences known. A key issue in the field is the characterization of preamyloid oligomers. The role of the C-terminus in amyloid formation is relatively unexplored, but recent solution NMR studies using recombinant human IAPP (hIAPP) strongly suggested that His-18 and Tyr-37 make early contacts during amyloid formation by an unamidated variant of IAPP at acidic pH (18). His-aromatic amino acid interactions are known to be important in globular proteins (19), but have not been widely considered in the context of amyloid formation, and it is not known if these interactions are formed in the naturally occurring amidated form of IAPP or whether they are important if present. A model of an antiparallel stable dimer generated by stacking of the side chains of His-18 and Tyr-37 was proposed based on the NMR studies (18). However, removal of the charged carboxylate and replacement with a neutral amide group to generate the physiological form of IAPP could alter interactions with the His side chain. In addition, the interactions involving His-18 and a charged C-terminus should be weaker at physiological pH because the pKa of His-18 is expected to be near, or below 7 in the monomeric state. Thus, the fraction of peptide with a protonated His-18 will decrease as the pH rises to physiological valves. Along these lines, previous studies of C-terminus amidated IAPP variants that contain the fluorescent Tyr/Phe analog 4-cyanophenylalanine argued that the aromatic side chains remain solvated during the lag phase and suggested that aromatic-aromatic interactions involving Tyr-37 or interactions of Tyr-37 with a neutral His do not develop during the lag time (20). Other models of low order oligomers have been proposed; including, for example, the formation of helical intermediates or the generation of dimers involving a side-by-side arrangement of β-hairpin monomers (21–25). Thus, the role of potential His-18-Tyr-37 interactions is not clear, and the role of C-terminus in amyloid formation is not completely defined, nor is the nature of early structure acquisition clear. These issues are important because some inhibitors may target early oligomeric structures, and because oligomeric intermediates are

Submitted November 6, 2013, and accepted for publication December 27, 2013.

*Correspondence: daniel.raleigh@stonybrook.edu

Editor: David Eliezer.

0006-3495/14/04/1520/8 $2.00

http://dx.doi.org/10.1016/j.bpj.2013.12.052

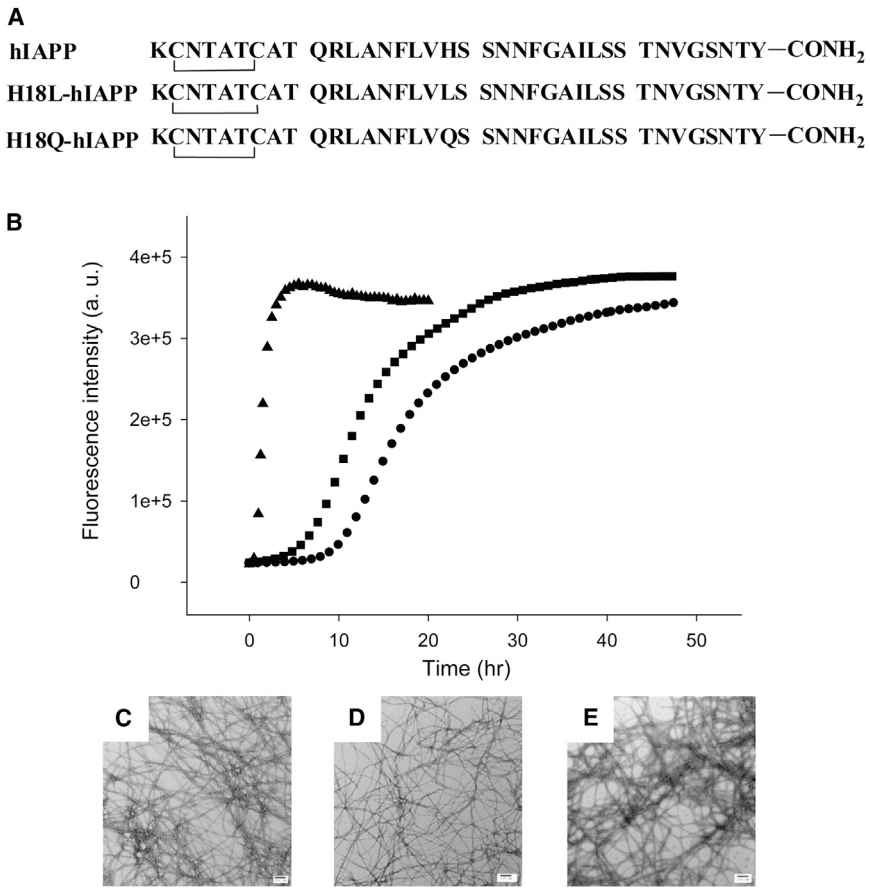

FIGURE 1 (*A*) Primary sequence of hIAPP and the two IAPP variants designed to study the potential His-18, Tyr-37 interaction in the naturally occurring amidated background. All peptides contain a disulfide bridge between residues 2 and 7, and an amidated C-terminus. (*B*) ThT fluorescence monitored kinetic experiments. Dots, hIAPP; Squares, H18Q-hIAPP; Triangles, H18L-hIAPP. All experiments were conducted in 20 mM, pH 7.4 Tris buffer, without stirring at 25°C. (*C*) TEM image of the amyloid fibrils formed by hIAPP. (*D*) TEM image of the amyloid fibrils formed by H18Q-hIAPP. (*E*) TEM image of the amyloid fibrils formed by H18L-hIAPP. Scale bars represent 100 nm.

thought to be the most toxic species (10,13,26–28). Here, we investigate the role of the C-terminus of IAPP and its interaction with His-18 during amyloid formation by IAPP.

MATERIALS AND METHODS

Peptide synthesis and purification

Peptides were synthesized on a 0.1 mmol scale using a CEM Liberty microwave peptide synthesizer, and 9-fluornylmethoxycarbonyl (Fmoc) chemistry. Solvents used were ACS-grade. 5-(4′-fmoc-aminomethyl-3′, 5-dimethoxyphenol) valeric acid (PAL-PEG-PS) resin was used to form an amidated C-terminus. Fmoc-L-Tyr (*Ot*Bu)-PEG-PS resin was used for the preparation of peptides with a free C-terminus. Standard Fmoc reaction cycles were used. Fmoc protected pseudoproline dipeptide derivatives were incorporated at positions 9–10, 19–20, and 27–28 to facilitate the synthesis (29). The β-branched residues, Arg, and all pseudoproline dipeptide derivatives were double coupled. A maximum temperature of 50°C was used for the coupling of His and Cys to reduce the possibility of racemization (30). Peptides were cleaved from the resin by standard trifluoroacetic acid (TFA) methods. Crude peptides were partially dissolved in 20% acetic acid (v/v), frozen in liquid nitrogen, and lyophilized to increase their solubility. The dry peptide was redissolved in dimethyl sulfoxide at room temperature to promote the formation of the disulfide bond (31,32). Peptides were purified by reverse-phase high-performance liquid chromatography using a Vydac or Proto 300 C18 preparative column (10 mm × 250 mm). A two buffer gradient was used: buffer A consisted of 100% H_2O and 0.045% HCl (v/v) and buffer B included 80% acetonitrile, 20% H_2O, and 0.045% HCl. HCl was used as the counterion instead of TFA because residual TFA can influence amyloid formation. Analytical high-performance liquid chromatography was used to check the purity of peptides before use. Matrix-assisted laser desorption/ionization time of flight mass spectrometry confirmed the correct molecular mass. hIAPP, expected 3903.3, observed 3902.8; H18Q-hIAPP, expected 3894.3, observed 3894.4; H18L-hIAPP, expected 3879.3, observed 3879.3; free CT-hIAPP, expected 3904.2, observed 3903.8; free H18Q CT-IAPP, expected 3895.3, observed 3895.9.

Sample preparation

Peptides were dissolved in 100% hexafluoroisopropanol at a concentration of 1.6 mM and stored at −20°C. For kinetic studies, 8 μL aliquots were lyophilized and redissolved in 800 μL of 20 mM Tris-HCl buffer, pH 7.4. For the seeding assays, preformed fibrils were produced from kinetic studies. The solution was incubated and ThT fluorescence was monitored to ensure that fibril formation had occurred. Seeds were freshly prepared to ensure reproducibility.

ThT fluorescence assays

For kinetic assays, solutions were prepared by adding 20 mM, pH 7.4 Tris–HCl buffer containing ThT to lyophilized dry peptides for a final peptide concentration of 16 μM. For the seeding assays, preformed fibrils mixed with Tris-HCl buffered ThT solution were added to the lyophilized dry hIAPP samples. The final condition was 16 μM peptide, 32 μM ThT, 1.6 μM seeds (in monomer units), and 20 mM Tris-HCl at pH 7.4. Measurements were made at 25°C using a Beckman Coulter DTX880 plate reader without stirring.

Transmission electron microscopy (TEM)

TEM was performed at the Life Science Microscopy Center at Stony Brook University. Aliquots were removed from the same solutions that were used for the fluorescence measurements. 5 μL of peptide solution was placed on a carbon-coated Formvar 300 mesh copper grid for 1 min and then negatively stained with saturated uranyl acetate for another 1 min.

Two-dimensional infrared spectroscopy (2DIR)

Samples for 2DIR were prepared at 0.5 mM in 20 mM pH 7.4 Tris-HCl buffer in D_2O, in a CaF_2 infrared cell with a 56 μm Teflon spacer, after overnight deuterium exchange in 100% hexafluoroisopropanol-d (Aldrich). 2DIR spectra were collected as described previously (33). Briefly, 60 fs mid-IR pulses centered at 6 μm, generated by optical parametric amplification of light from a regeneratively amplified Ti: sapphire laser system, were split into pump and probe beams, the former of which was sent through a Ge-based mid-IR acoustooptic pulse shaper to generate the pump pulse pair needed for 2D spectra and to provide shot-to-shot phase cycling. After passing through the excitation region of the pump beam, the probe beam was detected and digitized with a 64 element MCT detector array system (Infrared Systems). The pump and probe beams were polarized parallel in all experiments.

RESULTS AND DISCUSSION

Design of a model system to study the role of His-18 and Tyr-37 interactions in IAPP amyloid formation

The primary sequence of hIAPP is shown in Fig. 1 *A*. The molecule contains a single histidine at position 18 and three aromatic residues, including a single tyrosine at the C-terminus. Several structural models of hIAPP amyloid fibrils have been proposed; one based on the analysis of small peptide fragments of hIAPP and two based on solid-state NMR studies (34,35). His-18 is buried in the core of the fibril in the model based on crystallographic studies, and in one of the NMR-based models. However, calculations performed at the level of the linearized Poisson-Boltzmann equation argue that the network of interactions formed by His-18 is enough to overcome the desolvation barrier for a neutral His side chain (36). The C-terminal Tyr is part of the ordered β-sheet core in all models and the parallel in register β-structure mean that the C-terminus of the one polypeptide chain is close to the C-terminus of its neighbors. Thus, there should be considerable charge repulsion in amyloid fibrils formed from variants with a free C-terminus, provided of course that they adopt the same structure.

To investigate the potential importance of His-18 and Tyr-37 interactions, we synthesized hIAPP variants in which His-18 was replaced by the neutral residues, Gln and Leu. These substitutions were chosen because they are roughly similar in volume to His. Obviously, they differ in shape and hydrophobicity and these factors could influence amyloid formation. However, the use of two different substitutions at position 18 helps to ensure that any conclusions are robust. Additional variants were prepared with a free C-terminus and substitutions at position-18. (Fig. 1 *A* and Fig. 2 *A*). The rate of amyloid formation was measured using fluorescent detected ThT binding assays. ThT is a small dye whose quantum yield is enhanced when it binds to amyloid fibrils (37). ThT assays accurately report on IAPP amyloid formation kinetics and the presence of the dye does not alter the kinetics under the conditions used here (38).

The data collected for hIAPP show a typical sigmoidal curve with a lag phase followed by a growth phase and then a steady state in which soluble peptide is in equilibrium with amyloid fibrils (Fig. 1 *B*, *dots*). The H18Q-hIAPP single mutant forms amyloid fibrils moderately faster than hIAPP (Fig. 1 *B*, *squares*) and the fibril morphology is similar to hIAPP fibrils as judged by TEM and 2DIR (Fig. 1, *C* and *D*, and Fig. 3). This argues that any interactions between His-18 and the C-terminus Tyr are not critical for amyloid formation because their disruption at physiologically relevant pH does not inhibit amyloid formation, but actually accelerates it. When His-18 is replaced by Leu, a less polar substitution than Gln, even more dramatic effects are observed and amyloid formation is much faster. No apparent lag phase is observed for H18L-hIAPP (Fig. 1 *B*, *triangles*). The protonated state of His-18 significantly affects the rate of amyloid formation (39), however the pH used in these studies is 7.4 ± 0.2, and His-18 is expected to be largely deprotonated under these conditions. Hence, the effects are unlikely to be due simply to removal of a positive charge.

IAPP variants with a free C-terminus behave differently than C-terminal amidated IAPP

Previous work has shown that the natural amidated form of hIAPP and an IAPP variant with a free acid at its C-terminus form a different distribution of oligomers during the aggregation process (40), but putative His-18 and Tyr-37 interactions have not been probed.

To examine the possible role of interactions between His-18 and the C-terminus, we synthesized variants of hIAPP with a free acid C-terminus (denoted free CT-hIAPP, Fig. 2 *A*). This is the same form that was used in the solution NMR studies that defined the head-to-tail dimers (18). Free CT-hIAPP formed amyloid much more slowly than hIAPP, by a factor of 4, as judged by the t_{50} value of the two kinetic profiles (Fig. 2 *B*, *dots and squares*). The t_{50} is defined as the time required for 50% of the signal change in a ThT experiment. TEM images revealed differences in fibril morphology. hIAPP formed long and dense fibrils, whereas the free CT-hIAPP fibrils are shorter and curly (Fig. 2, *C* and *D*). We also prepared an hIAPP variant with a free acid C-terminus and a His-to-Gln substitution (denoted H18Q free CT-IAPP, Fig. 2 *A*) to analyze the impact of replacing His-18 in the free carboxylate background. H18Q free CT-IAPP formed amyloid faster than free CT-hIAPP

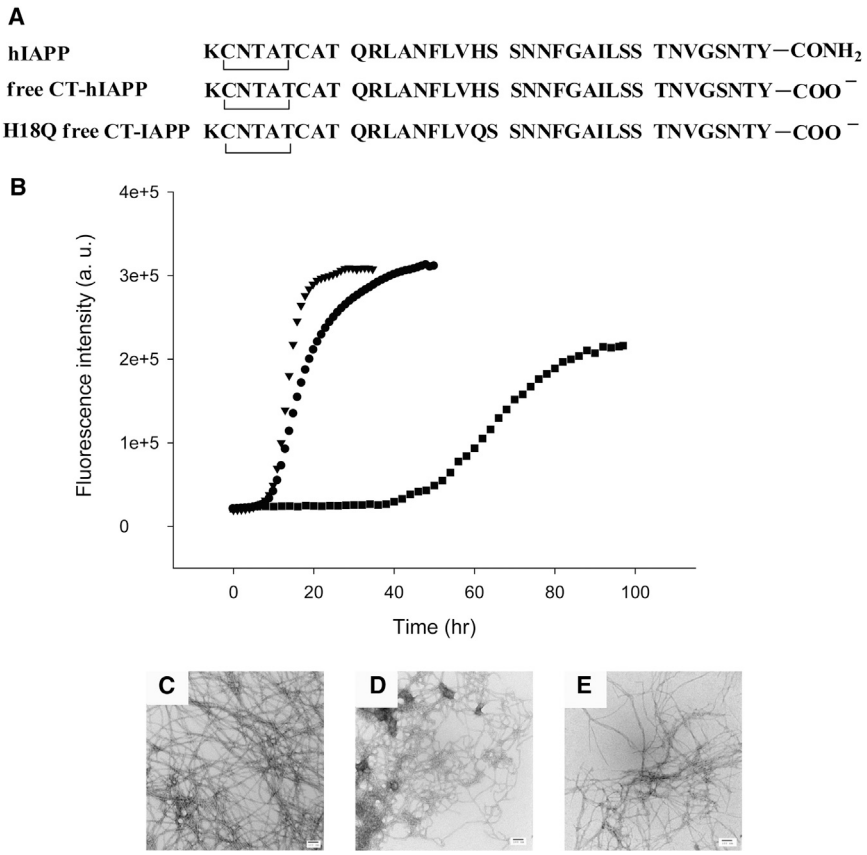

FIGURE 2 (*A*) Primary sequence of hIAPP and the two IAPP variants with a free C-terminus. All peptides contain a disulfide bridge between residues 2 and 7. (*B*) ThT fluorescence monitored kinetic experiments. Dots, hIAPP; Triangles, H18Q free CT-IAPP; Squares, free CT-hIAPP. All experiments were conducted in 20 mM, pH 7.4 Tris buffer, without stirring at 25°C. (*C*) TEM image of the amyloid fibrils formed by hIAPP. The micrograph is the same as the one shown in Fig. 1. (*D*) TEM image of the amyloid fibrils formed by free CT-hIAPP. (*E*) TEM image of the amyloid fibrils formed by H18Q free CT-IAPP. Scale bars represent 100 nm.

(Fig. 2 *B*, *triangles and squares*). Again, the data show that replacement of His-18 accelerates amyloid formation and thus indicates that His-18-Tyr-37 interactions are not essential for amyloid formation in either background at pH 7.4.

We used 2DIR to probe the secondary structure of amyloid fibrils formed by the different variants. The IR transitions of the Amide-I′ modes of proteins are sensitive to secondary structure and 2DIR has been used to monitor secondary structure as well as the packing of individual peptides in IAPP amyloid (41,42). 2DIR spectra were recorded for all of the samples and are displayed in Fig. 3. The spectra are broadly similar to previously reported spectra of hIAPP (42). The slice along the diagonal in the 2DIR contains similar information to a traditional linear IR spectrum, but with more prominent β-sheet signal because β-sheets and α-helices have stronger transitions

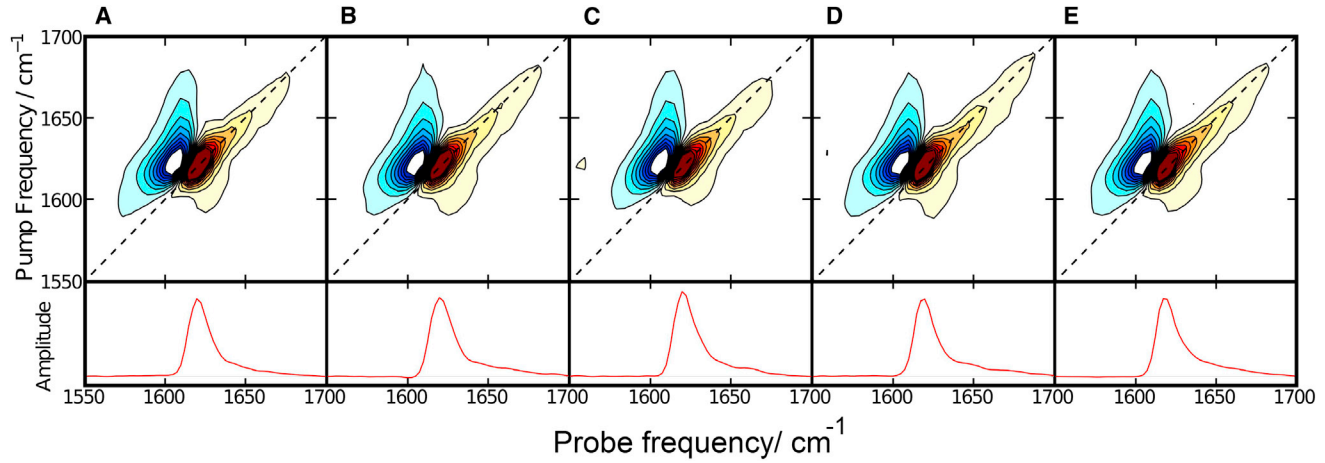

FIGURE 3 Two-dimensional infrared spectroscopy confirms that all peptides form amyloid fibrils. (*A*) hIAPP. (*B*) H18L-hIAPP. (*C*) H18Q-hIAPP. (*D*) Free CT-hIAPP. (*E*) H18Q free CT-IAPP. The diagonal slices of each spectrum are shown at the bottom of the figure. To see this figure in color, go online.

than random coils in 2D IR spectra (43) The diagonal slices are very similar and all display a prominent, sharp peak centered near 1617–1620 cm^{-1}, a frequency range that corresponds to β-structure. The data show that all of the variants form β-sheet-rich aggregates.

Nonadditive effects are observed with multiple mutations

hIAPP with a free C-terminus formed amyloid significantly more slowly than wild-type (WT) hIAPP with a fourfold longer t_{50}, whereas the His-to-Gln mutation at position 18 slightly accelerated the process (~20%). If the effects of the changes are independent there should be no synergy between them and the effect of a double mutation should be the sum of the individual effects. This approach is widely used in studies of protein folding and protein stability where the processes under consideration can usually be described by simple models using a limited number of thermodynamic states (44). Amyloid formation is significantly more complex and may involve multiple pathways and heterogeneous distributions of intermediates. In addition, it is presently impossible to measure rate constants for each of the microscopic steps in amyloid formation and, instead, t_{50} or the lag time is often used as a proxy for the time constant. However, t_{50} and the lag time likely cannot be related to the lifetime of a single kinetic step. These considerations indicate that there are considerable complications in using a double mutant cycle type approach to analyze amyloid kinetics, nonetheless, a semiquantitative analysis can still provide insight. If $1/t_{50}$ is used as a proxy for the rate, i.e., t_{50} is used as a proxy for an individual time constant, then one expects additive effects on the value of $\ln(1/t_{50})$ if two substitutions are independent, or equivalently, multiplicative effects on $(1/t_{50})$. Here, we used the ratio $(t_{50}/t_{50\text{-WT}})$ where $t_{50\text{-WT}}$ is the t_{50} of normal amidated WT hIAPP. The expected additive effect was estimated by multiplying this parameter (t_{50} of single mutant/ $t_{50\text{-WT}}$) calculated for the two single substitutions. The analysis revealed that the observed effects were not equal to the result expected for noninteracting sites (Fig. 4). The t_{50} for H18Q free CT-IAPP is 0.8 that of hIAPP, whereas the expected result, assuming independent effects, is 3.2-fold. This analysis suggests that the C-terminal carboxylate interacts with His-18, but that the interaction does not favor amyloid formation.

Amyloid fibrils formed by IAPP variants with a free acid C-terminus do not seed amyloid formation by hIAPP

We further examined the structural similarity between hIAPP fibrils and the fibrils formed by different hIAPP variants using seeding experiments. Preformed hIAPP fibrils can be used as seeds to seed amyloid formation by monomeric hIAPP leading to a bypassing of the lag phase. Seeding is generally specific and structural differences between different proteins impact seeding efficiencies (45,46).We first seeded hIAPP with hIAPP fibrils as a control. As expected, a bypass of the lag phase was observed and a significant increase in ThT fluorescence in the first few hours was detected (Fig. 5, *open circles*). We then tested the ability of fibrils formed by the different variants to seed hIAPP. When hIAPP was seeded by preformed H18Q-hIAPP fibrils, a curve similar to the control study was observed, suggesting that H18Q- hIAPP formed fibrils that are very similar to those generated by hIAPP fibrils (Fig. 5, *diamonds*). In striking contrast, either of the variants with a free C-terminus is much less effective at seeding amyloid formation by hIAPP and a significant lag phase is still observed. (Fig. 5, *squares and triangles*). This result highlights the importance of the C-terminus and strongly suggests that there are differences in the details of the fibril

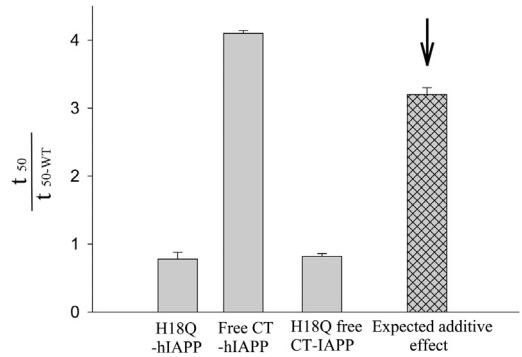

FIGURE 4 Nonadditive effects were observed between the C-terminus and His-18. The histogram shows the effect caused by mutation or by modification of the C-terminus. The expected additive result is indicated by the arrow.

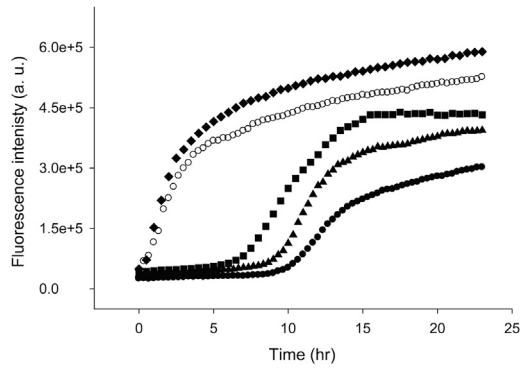

FIGURE 5 Amyloid fibrils formed by IAPP variants with a free acid C-terminus are much less effective at seeding amyloid formation by hIAPP than amyloid fibrils formed by variants with an amidated C-terminus. ThT fluorescence monitored kinetic experiments: Dots, unseeded hIAPP; Open circles, hIAPP seeded by hIAPP amyloid fibrils; Diamonds, hIAPP seeded by H18Q-hIAPP amyloid fibrils; Triangles, hIAPP seeded by free CT-hIAPP amyloid fibrils; Squares, hIAPP seeded by free H18Q CT-IAPP amyloid fibrils. Seeds were present at 10% concentration in monomer units.

structure formed by amidated and unamidated hIAPP. It is striking that simply replacing an amide group at the C-terminus by a carboxylate has more effect than replacing His-18 by residues that differ significantly in shape and polarity.

Analysis of H18Q-hIAPP reveals that the protonation state of the N-terminus affects the rate of amyloid formation

The rate of hIAPP amyloid formation is pH dependent and is faster above pH 7 than below. This is likely due in part to the deprotonation of His-18, but the free N-terminus could also contribute (39,47). Our H18Q-hIAPP mutant allows us to probe the role of the protonation state of the N-terminus in a background where no other groups titrate with a similar pKa. Amyloid formation by the mutant is approximately fourfold faster at pH 7.5 relative to the rate at pH 5.0 (Fig. 6, Fig. S2). The data highlight the contribution of the N-terminal charge state to amyloid formation and reveals that the pKa of the free N-terminus is below 7.5. All models of IAPP amyloid fibril postulate that the N-terminus is flexible, thus the strong dependence of the rate of amyloid formation on its charge state is striking.

CONCLUSIONS

The analysis presented here clearly shows that interactions involving His-18 and the C-terminus Tyr are not essential for amyloid formation and, furthermore, show that disrupting this potential interaction in both backgrounds enhances the rate of amyloid formation. Previous work, using recombinant IAPP with a free C-terminus, provided good evidence, via NMR, for interactions between His-18 and the C-terminus at pH 5.5 (18). This led to a model for formation of a head-to-tail dimer. Such interactions are expected to be stronger in the IAPP variant with a free C-terminus at low pH because the negatively charged carboxylate will make stronger interactions with His-18, which will be positively charged at pH 5.5. The data presented here show that if such interactions are formed in the physiologically relevant amidated form at physiological pH they do not promote amyloid formation, but rather hinder it.

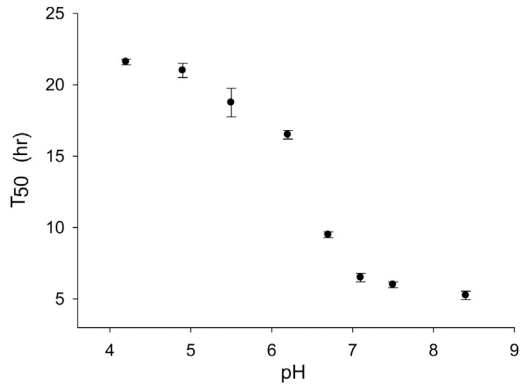

FIGURE 6 The pH dependence of amyloid formation by H18Q-hIAPP shows that the charge state of the N-terminus plays an important role in amyloid formation. Values of t_{50} are plotted versus pH. Experiments were conducted at 25°C in 20 mM Tris. The error bars were derived by conducting 3 to 4 independent measurements for each pH. The pH was adjusted by addition of small amounts of HCl. The maximum added Cl^-, beyond that present in the Tris buffer, due to the addition of HCl was 5 mM.

Does this mean that the C-terminus of IAPP does not interact with the side chain of His-18? Not necessarily. The observation of nonadditive effects between the C-terminus and His-18 is consistent with formation of an interaction, although the effects are small. However, this does not imply that head-to-tail dimers are formed; they may be, but the fact that replacement of His-18 accelerates amyloid formation is broadly consistent with other models of early intermediates. The helical intermediate model predicts that the key contacts are made in the region of residues 8 to 18 and replacement of His might improve packing in this region (21–23). The β-hairpin model involves two intramolecular β-hairpins packing together via strand-strand interactions in the region of residues 11 to 18 and residues 23 to 32 (24). Again, replacement of His-18 could modify these interactions and might reduce unfavorable interactions between two polar side chains.

Replacement of the neutral amidated C-terminus with a negatively charged free carboxylate significantly decreased the rate of amyloid formation, consistent with previous studies (39), even though the change decreases the net charge on the polypeptide, showing that the rate of aggregation does not correlate with the net charge of the peptide although electrostatic interactions and peptide ion interactions are important in IAPP aggregation (36). There is a parallel with the solubility of globular proteins; to a rough first approximation, proteins are the least soluble when the pH equals the protein pI, but there are numerous examples where proteins are actually less soluble when pH does not equal the pI.

The fact that hIAPP variants with a free C-terminus are significantly less amyloidogenic argues that hIAPP is not under strong evolutionary pressure to minimize amyloidogenicity. The advantages of a modified C-terminus, enhanced resistance to proteases and possibly higher activity clearly outweigh the deleterious effects of increased in vitro amyloidogenicity. The likely explanations are that, until very recently, type 2 diabetes and islet amyloid did not significantly affect the young, thus prevention of islet amyloid was not under strong evolutionary pressure. A second, but not exclusive, possibly is that in vitro amyloidogenicity does not directly correlate with in vivo amyloidogenicity. The latter point may be relevant for hIAPP because hIAPP normally does not form amyloid in vivo even though it is stored in the secretary granule at concentrations that lead to rapid amyloid formation in vitro.

SUPPORTING MATERIAL

Two figures are available at http://www.biophysj.org/biophysj/supplemental/S0006-3495(14)00130-1.

We thank Mr. Bezalel A. Bacon for assistance with peptide purification, and Dr. Ping Cao for helpful discussions.

This work was supported by National Institutes of Health (NIH) grants GM078114 to D.P.R. and DK79895to M.Z.

The authors declare no conflict of interest.

REFERENCES

1. Selkoe, D. J. 2004. Cell biology of protein misfolding: the examples of Alzheimer's and Parkinson's diseases. *Nat. Cell Biol.* 6:1054–1061.
2. Chiti, F., and C. M. Dobson. 2006. Protein misfolding, functional amyloid, and human disease. *Annu. Rev. Biochem.* 75:333–366.
3. Lansbury, P. T., and H. A. Lashuel. 2006. A century-old debate on protein aggregation and neurodegeneration enters the clinic. *Nature.* 443:774–779.
4. Levine, H. 1995. Thioflavin-T interaction with amyloid beta-sheet structures. *Amyloid.* 2:1–6.
5. Cooper, G. J. S., A. C. Willis, …, K. B. M. Reid. 1987. Purification and characterization of a peptide from amyloid-rich pancreases of type 2 diabetic patients. *Proc. Natl. Acad. Sci. USA.* 84:8628–8632.
6. Clark, A., G. J. Cooper, …, R. C. Turner. 1987. Islet amyloid formed from diabetes-associated peptide may be pathogenic in type-2 diabetes. *Lancet.* 2:231–234.
7. Westermark, P., C. Wernstedt, …, K. H. Johnson. 1987. Amyloid fibrils in human insulinoma and islets of Langerhans of the diabetic cat are derived from a neuropeptide-like protein also present in normal islet cells. *Proc. Natl. Acad. Sci. USA.* 84:3881–3885.
8. Lorenzo, A., B. Razzaboni, …, B. A. Yankner. 1994. Pancreatic islet cell toxicity of amylin associated with type-2 diabetes mellitus. *Nature.* 368:756–760.
9. Hull, R. L., G. T. Westermark, …, S. E. Kahn. 2004. Islet amyloid: a critical entity in the pathogenesis of type 2 diabetes. *J. Clin. Endocrinol. Metab.* 89:3629–3643.
10. Westermark, P., A. Andersson, and G. T. Westermark. 2011. Islet amyloid polypeptide, islet amyloid, and diabetes mellitus. *Physiol. Rev.* 91:795–826.
11. Cao, P., A. Abedini, and D. P. Raleigh. 2013. Aggregation of islet amyloid polypeptide: from physical chemistry to cell biology. *Curr. Opin. Struct. Biol.* 23:82–89.
12. Cao, P., P. Marek, …, D. P. Raleigh. 2013. Islet amyloid: from fundamental biophysics to mechanisms of cytotoxicity. *FEBS Lett.* 587:1106–1118.
13. Abedini, A., and A. M. Schmidt. 2013. Mechanisms of islet amyloidosis toxicity in type 2 diabetes. *FEBS Lett.* 587:1119–1127.
14. Westermark, G. T., P. Westermark, …, A. Andersson. 2003. Formation of amyloid in human pancreatic islets transplanted to the liver and spleen of nude mice. *Ups. J. Med. Sci.* 108:193–203.
15. Westermark, G. T., P. Westermark, …, O. Korsgren; Nordic Network for Clinical Islet Transplantation 2008. Widespread amyloid deposition in transplanted human pancreatic islets. *N. Engl. J. Med.* 359:977–979.
16. Potter, K. J., A. Abedini, …, C. B. Verchere. 2010. Islet amyloid deposition limits the viability of human islet grafts but not porcine islet grafts. *Proc. Natl. Acad. Sci. USA.* 107:4305–4310.
17. Roberts, A. N., B. Leighton, …, G. J. S. Cooper. 1989. Molecular and functional characterization of amylin, a peptide associated with type 2 diabetes mellitus. *Proc. Natl. Acad. Sci. USA.* 86:9662–9666.
18. Wei, L., P. Jiang, …, K. Pervushin. 2011. The molecular basis of distinct aggregation pathways of islet amyloid polypeptide. *J. Biol. Chem.* 286:6291–6300.
19. Meurisse, R., R. Brasseur, and A. Thomas. 2003. Aromatic side-chain interactions in proteins. Near- and far-sequence His-X pairs. *Biochim. Biophys. Acta.* 1649:85–96.
20. Marek, P., R. Gupta, and D. P. Raleigh. 2008. The fluorescent amino acid *p*-cyanophenylalanine provides an intrinsic probe of amyloid formation. *ChemBioChem.* 9:1372–1374.
21. Abedini, A., and D. P. Raleigh. 2009. A critical assessment of the role of helical intermediates in amyloid formation by natively unfolded proteins and polypeptides. *Protein Eng. Des. Sel.* 22:453–459.
22. Abedini, A., and D. P. Raleigh. 2009. A role for helical intermediates in amyloid formation by natively unfolded polypeptides? *Phys. Biol.* 6:015005–015010.
23. Wiltzius, J. J. W., S. A. Sievers, …, D. Eisenberg. 2009. Atomic structures of IAPP (amylin) fusions suggest a mechanism for fibrillation and the role of insulin in the process. *Protein Sci.* 18:1521–1530.
24. Dupuis, N. F., C. Wu, …, M. T. Bowers. 2011. The amyloid formation mechanism in human IAPP: dimers have β-strand monomer-monomer interfaces. *J. Am. Chem. Soc.* 133:7240–7243.
25. Williamson, J. A., and A. D. Miranker. 2007. Direct detection of transient alpha-helical states in islet amyloid polypeptide. *Protein Sci.* 16:110–117.
26. Janson, J., R. H. Ashley, …, P. C. Butler. 1999. The mechanism of islet amyloid polypeptide toxicity is membrane disruption by intermediate-sized toxic amyloid particles. *Diabetes.* 48:491–498.
27. Klein, W. L., W. B. Stine, Jr., and D. B. Teplow. 2004. Small assemblies of unmodified amyloid beta-protein are the proximate neurotoxin in Alzheimer's disease. *Neurobiol. Aging.* 25:569–580.
28. Baglioni, S., F. Casamenti, …, M. Stefani. 2006. Prefibrillar amyloid aggregates could be generic toxins in higher organisms. *J. Neurosci.* 26:8160–8167.
29. Abedini, A., and D. P. Raleigh. 2005. Incorporation of pseudoproline derivatives allows the facile synthesis of human IAPP, a highly amyloidogenic and aggregation-prone polypeptide. *Org. Lett.* 7:693–696.
30. Marek, P., A. M. Woys, …, D. P. Raleigh. 2010. Efficient microwave-assisted synthesis of human islet amyloid polypeptide designed to facilitate the specific incorporation of labeled amino acids. *Org. Lett.* 12:4848–4851.
31. Tam, J. P., C. R. Wu, …, J. W. Zhang. 1991. Disulfide bond formation in peptides by dimethyl-sulfoxide -scope and applications. *J. Am. Chem. Soc.* 113:6657–6662.
32. Abedini, A., G. Singh, and D. P. Raleigh. 2006. Recovery and purification of highly aggregation-prone disulfide-containing peptides: application to islet amyloid polypeptide. *Anal. Biochem.* 351:181–186.
33. Middleton, C. T., A. M. Woys, …, M. T. Zanni. 2010. Residue-specific structural kinetics of proteins through the union of isotope labeling, mid-IR pulse shaping, and coherent 2D IR spectroscopy. *Methods.* 52:12–22.
34. Wiltzius, J. J., S. A. Sievers, …, D. Eisenberg. 2008. Atomic structure of the cross-beta spine of islet amyloid polypeptide (amylin). *Protein Sci.* 17:1467–1474.
35. Luca, S., W. M. Yau, …, R. Tycko. 2007. Peptide conformation and supramolecular organization in amylin fibrils: constraints from solid-state NMR. *Biochemistry.* 46:13505–13522.
36. Marek, P. J., V. Patsalo, …, D. P. Raleigh. 2012. Ionic strength effects on amyloid formation by amylin are a complicated interplay among Debye screening, ion selectivity, and Hofmeister effects. *Biochemistry.* 51:8478–8490.
37. LeVine, 3rd, H. 1993. Thioflavine T interaction with synthetic Alzheimer's disease beta-amyloid peptides: detection of amyloid aggregation in solution. *Protein Sci.* 2:404–410.
38. Marek, P., S. Mukherjee, …, D. P. Raleigh. 2010. Residue-specific, real-time characterization of lag-phase species and fibril growth during amyloid formation: a combined fluorescence and IR study of *p*-cyanophenylalanine analogs of islet amyloid polypeptide. *J. Mol. Biol.* 400:878–888.

39. Abedini, A., and D. P. Raleigh. 2005. The role of His-18 in amyloid formation by human islet amyloid polypeptide. *Biochemistry.* 44:16284–16291.

40. Chen, M. S., D. S. Zhao, …, Y. M. Li. 2013. Characterizing the assembly behaviors of human amylin: a perspective derived from C-terminal variants. *Chem. Commun. (Camb.).* 49:1799–1801.

41. Strasfeld, D. B., Y. L. Ling, …, M. T. Zanni. 2008. Tracking fiber formation in human islet amyloid polypeptide with automated 2D-IR spectroscopy. *J. Am. Chem. Soc.* 130:6698–6699.

42. Shim, S. H., R. Gupta, …, M. T. Zanni. 2009. Two-dimensional IR spectroscopy and isotope labeling defines the pathway of amyloid formation with residue-specific resolution. *Proc. Natl. Acad. Sci. USA.* 106:6614–6619.

43. Grechko, M., and M. T. Zanni. 2012. Quantification of transition dipole strengths using 1D and 2D spectroscopy for the identification of molecular structures via exciton delocalization: application to α-helices. *J. Chem. Phys.* 137:184202–184210.

44. Horovitz, A. 1996. Double-mutant cycles: a powerful tool for analyzing protein structure and function. *Fold. Des.* 1:R121–R126.

45. O'Nuallain, B., A. D. Williams, …, R. Wetzel. 2004. Seeding specificity in amyloid growth induced by heterologous fibrils. *J. Biol. Chem.* 279:17490–17499.

46. Krebs, M. R. H., L. A. Morozova-Roche, …, C. M. Dobson. 2004. Observation of sequence specificity in the seeding of protein amyloid fibrils. *Protein Sci.* 13:1933–1938.

47. Li, Y., W. X. Xu, …, J. Z. H. Zhang. 2013. Acidic pH retards the fibrillization of human Islet Amyloid Polypeptide due to electrostatic repulsion of histidines. *J. Chem. Phys.* 139:055102.

SUPPORTING INFORMATION

Mutational Analysis of Pre-Amyloid Intermediates: Critical Evaluation of the Role of His-Tyr Interactions in Islet Amyloid

Ling-Hsien Tu,† Arnaldo L. Serrano,‡ Martin T. Zanni,‡ and Daniel P. Raleigh,†*

† Department of Chemistry, Stony Brook University, Stony Brook, New York; ‡ Department of Chemistry, University of Wisconsin-Madison, Madison, Wisconsin

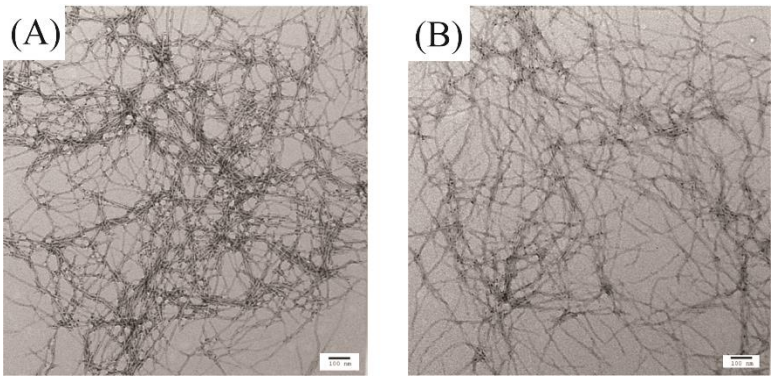

Figure S1: TEM images confirm the formation of amyloid fibrils. (A) hIAPP seeded by hIAPP amyloid fibrils. (B) hIAPP seeded by free CT-hIAPP amyloid fibrils. Aliquots were removed at the end of the seeding reactions shown in figure 5 of manuscript.

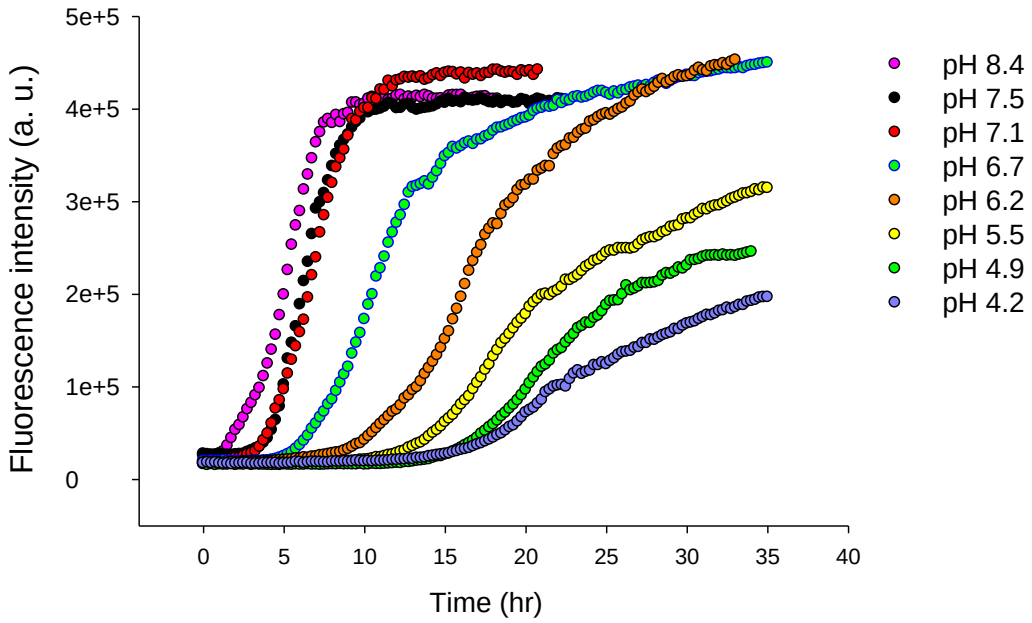

Figure S2: Thioflavin-T assays of the kinetics of amyloid formation by H18Q-hIAPP. The curves were used to measure the t_{50} values shown in figure 6 of the manuscript. Experiments were conducted at 25 ^{o}C. The peptide concentration was 20 uM.